Supporting Information (SI)

Air-con Metal–Organic Frameworks in Binder Composites for Water Adsorption Heat Transformation Systems

Serkan Gökpinar, [†] Sebastian-Johannes Ernst,[‡] Emrah Hastürk [†] Marc Möllers,[‡] Ilias El Aita [ǁ] Raphael Wiedey,[ǁ] Niels Tannert [†] Sandra Nießing,[†] Soheil Abdpour,[†] Alexa Schmitz,[†] Julian Quodbach,[ǁ] Gerrit Füldner,[‡] Stefan K. Henninger,[‡] and Christoph Janiak*[†]

[†] Institut für Anorganische Chemie und Strukturchemie and [ǁ] Institut für Pharmazeutische Technologie und Biopharmazie, Heinrich-Heine-Universität Düsseldorf, 40204 Düsseldorf, Germany
[‡] Fraunhofer Institut für Solare Energie Systeme (ISE), Heidenhofstr. 2, 79110 Freiburg, Germany.
*Email: serkan.goekpinar@uni-duesseldorf.de; sebastian-johannes.ernst@ise.fraunhofer.de; emrah.hastuerk@uni-duesseldorf.de; marc_moellers@web.de; elaita@uni-duesseldorf.de; raphael.wiedey@uni-duesseldorf.de; niels.tannert@hhu.de; Sandra.Niessing@uni-duesseldorf.de; abdpoursohail@gmail.com; alexa.schmitz@uni-duesseldorf.de; julian.quodbach@uni-duesseldorf.de; gerrit.fueldner@ise.fraunhofer.de; stefan.henninger@ise.fraunhofer.de; janiak@uni-duesseldorf.de

---

Contents

Section S1. N_2-Sorption Isotherms of MOF Powder and MOF Pellet

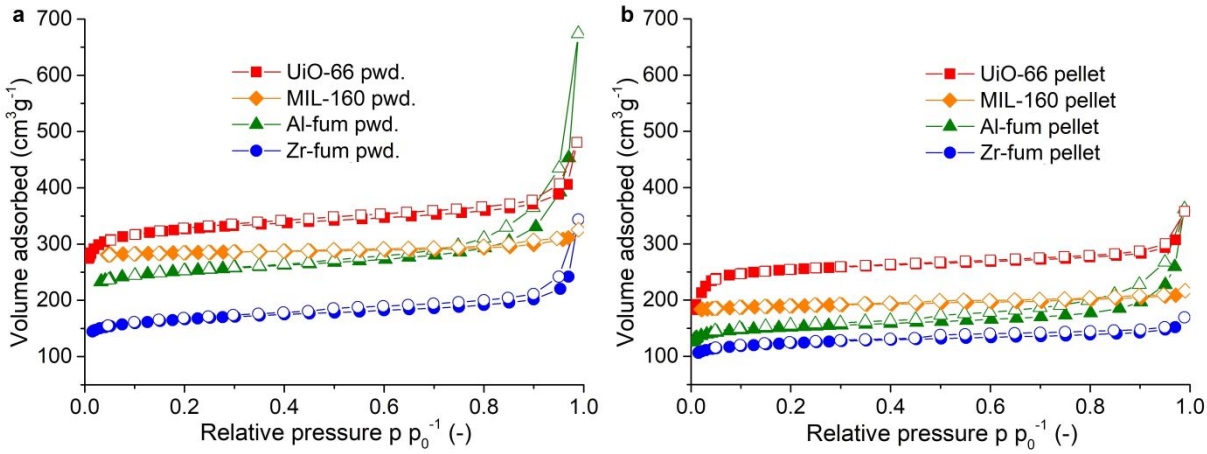

Figure S1 N_2 sorption isotherms of MIL-160, Al-fum, Zr-fum and UiO-66 a) powder and b) pellets. Filled symbols adsorption; empty symbols desorption.

Table S1. Micropore analysis of samples according to the V-t method.

Sample	Micropore SA [m^2/g] (% of calc. SA [a])	External SA [m^2/g] (% of calc. SA [a])	Micropore volume [$cm^3 \cdot g^{-1}$] (% of calc. micropore volume [b])
MIL-160(Al)	1095	28	0.428
MIL-160(Al) pellet	825 (94)	41 (156)	0.276 (78)
Al-fum	870	118	0.338
Al-fum pellet	517 (74)	78 (79)	0.201 (71)
Zr-fum	544	100	0.214
Zr-fum pellet	410 (93)	69 (82)	0.162 (88)
UiO-66(Zr)	1166	128	0.450
UiO-66(Zr) pellet	941 (100)	91 (86)	0.354 (95)

[a] calculated as the sum of the mass-weighted areas of the MOF and PVA from the following formula, respectively: $SA_{calc.} = SA_{MOF}$ x wt% MOF + SA_{PVA} x wt% PVA with wt% MOF = 0.8, wt% MOF= 0.2, $SA_{micropore} = 27\ m^2/g$, $SA_{external} = 19\ m^2/g$; [b] calculated as the sum of the mass-weighted micropore volume of the MOF and PVA from the following formula, respectively: $V_{micropore\ calc.} = V_{MOF,micropore}$ x wt% MOF + $V_{PVA,micropore}$ x wt% PVA with $V_{PVA,micropore} = 0.06\ cm^3/g$.

Section S2. Structure of Used MOFs

UiO-66 (UiO = University in Oslo), firstly synthesized by Lillerud and co-workers, is consisted of a $\{Zr_6O_4(OH)_4\}$-SBU, twelvefold coordinated by the linker molecule benzene-1,4-dicarboxylate linkers (BDC) resulting in a face-centered cubic (fcc) packing arrangement (see Fig. S2).[1] While UiO-66 has BDC as linker, the isoreticular MOF-801/**Zr-fumarate** is coordinated by fumaric acid.[2] The properties of these Zr-MOFs are interesting for gas storage,[3] separation,[4] water sorption,[5,6] sensing[7] and catalysis.[8]

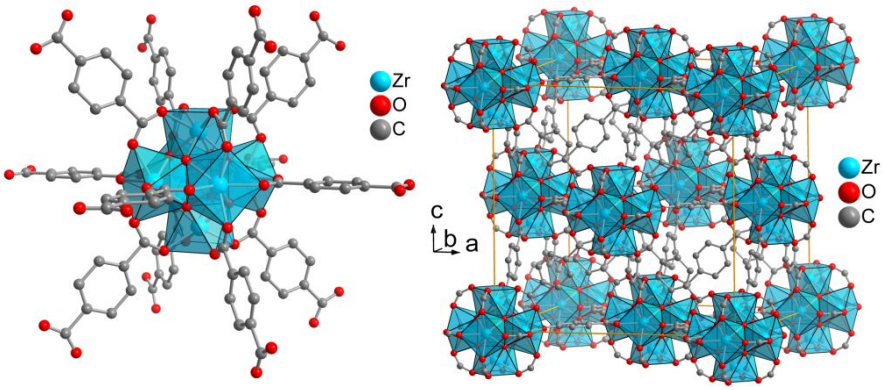

Figure S2 Crystal structure of zirconium terephthalate UiO-66. Hydrogen atoms and solvent molecules are not shown. The UiO-66 structure is drawn with the software Diamond from the deposited cif-file under CCDC no. 837796.[9] Zr-fum has an isoreticular structure, while linker terephthalate is replaced by fumarate.

Al-fumarate, described in the patent literature,[10] is one of the most promising MOFs for cooling applications due to its water based synthesis, inexpensive and benign metal cation and high stability.[6] The framework with the chemical formula $\{Al(OH)(fum) \cdot n\ H_2O\}_m$ is built up from Al-OH-Al chains connected by fumarate linkers resulting in lozenge-shaped 1D pores (see Fig. S3 left).[11] Further, a novel and very promising candidate is **MIL-160**, firstly synthesized by Cadiau *et al.*[12] It consists of helical cis corner-sharing chains of $AlO_4(OH)_2$ octahedra connected by 2,5-furandicarboxylate groups, building one dimensional square-shaped sinusoidal channels (see Fig. S3 right).[13]

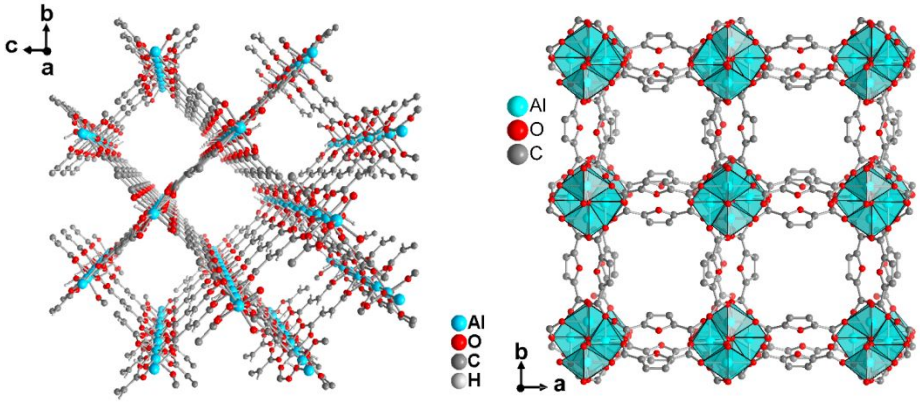

Figure S3 left: Crystal structure of aluminum fumarate. Graphic produced by software Diamond from cif-file for Basolite A520 (CCDC no. 1051975).[11]; right: Crystal structure of MIL-160. Graphic produced by software Diamond from cif-file under CCDC no. 1828695.[14]

Section S3. Summary of MOFs Before and After Shaping by Various Shaping Methods

MOF composite bodies using poly(vinylalcohol) (PVA) as a binder are known. Kim *et al.* produced PVA based granules of UiO-66 with a MOF-loading of ~78 wt% by using an extruder, synthesized for catalytic and gas storage application.[15] Khabzina *et al*. produced PVA and polysiloxane based UiO-66-COOH bodies for NH_3 air purification filters by using extrusion and freeze granulation technique.[16] Just to mention a few more shaping examples, Valekar *et al.* synthesized MIL-100(Fe), MIL-101(Cr), UiO-66(Zr) and UiO-66(Zr)-NH_2 MOF granules using the wet granulation method with 5 wt% mesoporous r-alumina (MRA) as binder.[17] The calculated BET surface areas varied from 92 to 98 % of the dry powders' value (calculation in Electronic Supplementary Information Section S3) and the average crushing strengths varied between 2.5 and 6.7 N. These MOF bodies were also tested for NH_3 adsorption and gas separation applications. Recently, Permyakova *et al.* produced MIL-160(Al) granules through wet-granulation method using silica sol as binder (10 wt%), with a size distribution of 0.5-1.8 mm.[13] This MOF, including the granules are very promising for water sorption application. Further, Lenzen *et al.* reported coatings and monoliths based on CAU-10-H MOF using the water based SilRes MP50E binder for use in adsorption-driven chiller systems. The pore accessibility for water molecules are fully retained, while the water uptake is reduced in equivalent to the amount of binder.[18]

Table S2. Summary of porous properties of MOFs before and after shaping by various shaping methods. Table taken from Valekar *et al.*, modified and supplemented with own results.[17]

MOF	Additives	Shaped body	BET Surface area (m^2/g)			Ref.
			Powder	Shaped body	% of calc. SA[d]	
MIL-100(Fe)	5% mesoporous r-alumina (MRA)	Granules	2088	1831	92	17
MIL-101(Cr)	5% MRA	Granules	4066	3685	95	17
UiO-66(Zr)	5% MRA	Granules	1050	911	90	17
UiO-66(Zr)-NH_2	5% MRA	Granules	875	823	98	17
UiO-66(Zr)	10% Sucrose [a]	Spheres	1367	674	≤55 [e]	19
UiO-66(Zr)	1% Graphite [b]	Pellets	1140	885	≤78 [e]	20
UiO-66(Zr)	23-33% Polyurethane [c]	Foam	1175	511-427	≤56-≤54 [e]	21
ZIF-8	20-50 Polysulfone [c]	Spheres	1023	761-128	≤93- ≤25 [e]	22
MIL-160	**20 % PVA**	**Pellets**	**1122**	**866**	**96**	o. w.
Al-fum	**20 % PVA**	**Pellets**	**988**	**595**	**74**	o. w.
Zr-fum	**20 % PVA**	**Pellets**	**643**	**479**	**91**	o. w.
UiO-66(Zr)	**20 % PVA**	**Pellets**	**1295**	**1031**	**99**	o. w.

[a] granulation; [b] pressing; [c] composite mixture shaping methods; [d] – SA calculated as the sum of the mass-weighted areas of the MOF and PVA from the following formula, respectively: $SBET_{calc.} = SBET_{MOF}$ x wt% MOF + $SBET_{PVA}$ x wt% PVA with $SBET_{PVA}$ = 48 m^2/g, $SBET_{MRA}$ = 218 m^2/g; [e] SBET of binder is not given and is set to 0 m^2/g to calculate the maximum.

Section S4. Heat of Adsorption Calculations for Pellets

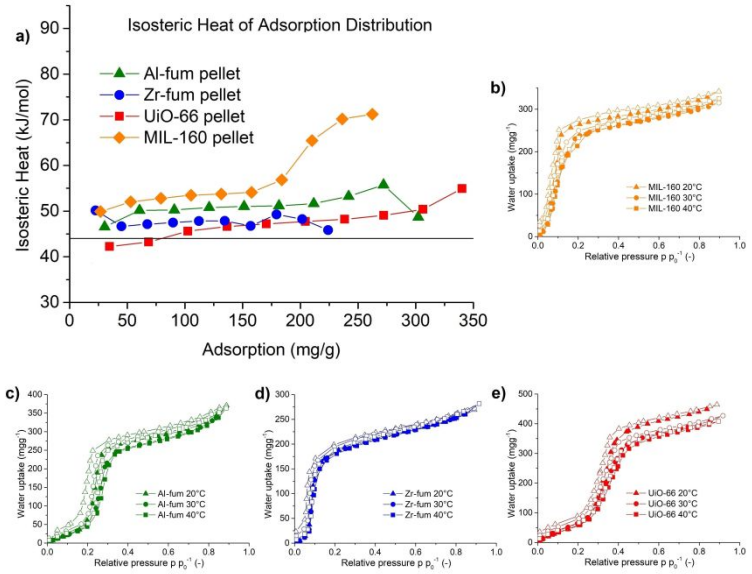

Figure S4 a) Heat of adsorption calculations of MIL-160, Al-fum, Zr-fum and UiO-66 pellets and volumetrically measured water sorption isotherms at different temperatures (20 °C, 30 °C and 40 °C) of b) MIL-160, c) Al-fum, d) Zr-fum and e) d) UiO-66 pellets.

Small deviations in Q_{st} are within the error margin of at least ±10 kJ/mol which can be assumed on average for Q_{st} data points.[23,24] Consequently Q^0_{st} values should not be reported or discussed with decimal digits. The calculated increase in Q_{st} with H_2O uptake can be to a simultaneous, exothermic process such as the rearrangement of already adsorbed H_2O molecules towards a closer, energetically more favorable configuration or a phase transition of the material. In a recent molecular dynamics simulation of H_2O adsorption in the Al-MOF CAU-10-H it was found that the first water molecules are primarily adsorbed in the proximity of the AlO_6 polyhedra via hydrogen bonding to the bridging OH groups and the carboxylate oxygen groups. As loading increases, the water-water interactions dominate as a result of the inter-water hydrogen bonding, giving rise to water clusters which may exert steric effects on the framework which leads to a distortion of the CAU framework.[25]

Section S5. Mechanical Stability Tests

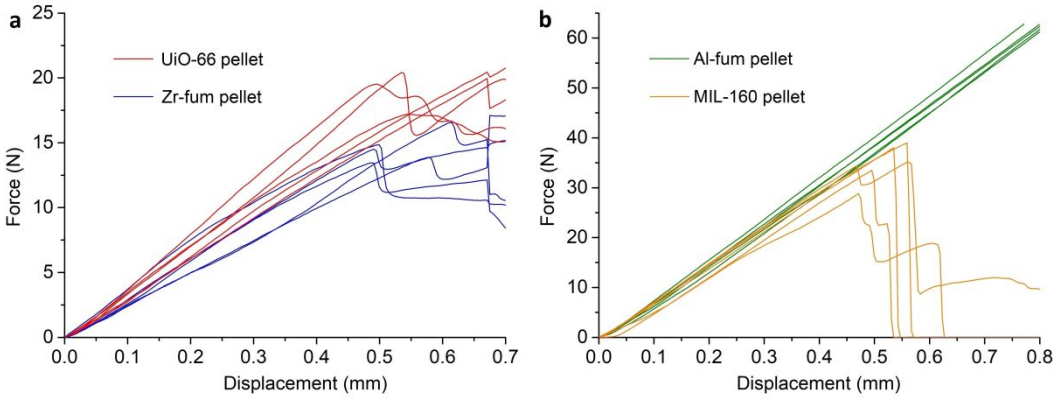

Figure S5 Mechanical stability tests of a) Zr-fum and UiO-66, b) MIL-160 and Al-fum pellets. All values higher than 63 N are measured by Erweka TBH210. For a better overview only 5 curves are shown.

Section S6. SEM Images

MIL-160

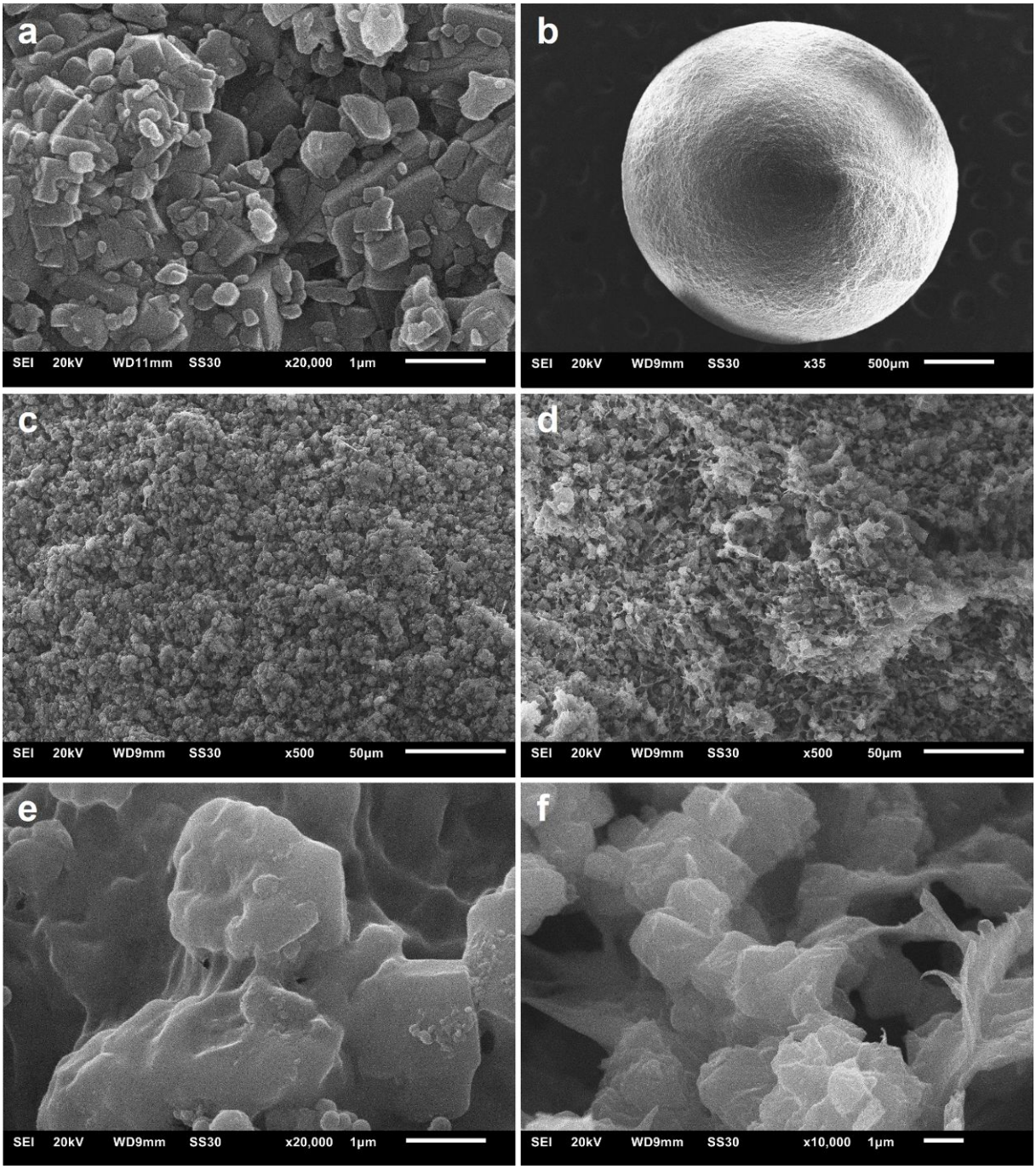

Figure S6 SEM pictures of MIL-160 powder (a), overview of MIL-160 pellet (b), surface of MIL-160 pellet (c, e) and cross section of MIL-160 pellet (d, f).

Al-fum

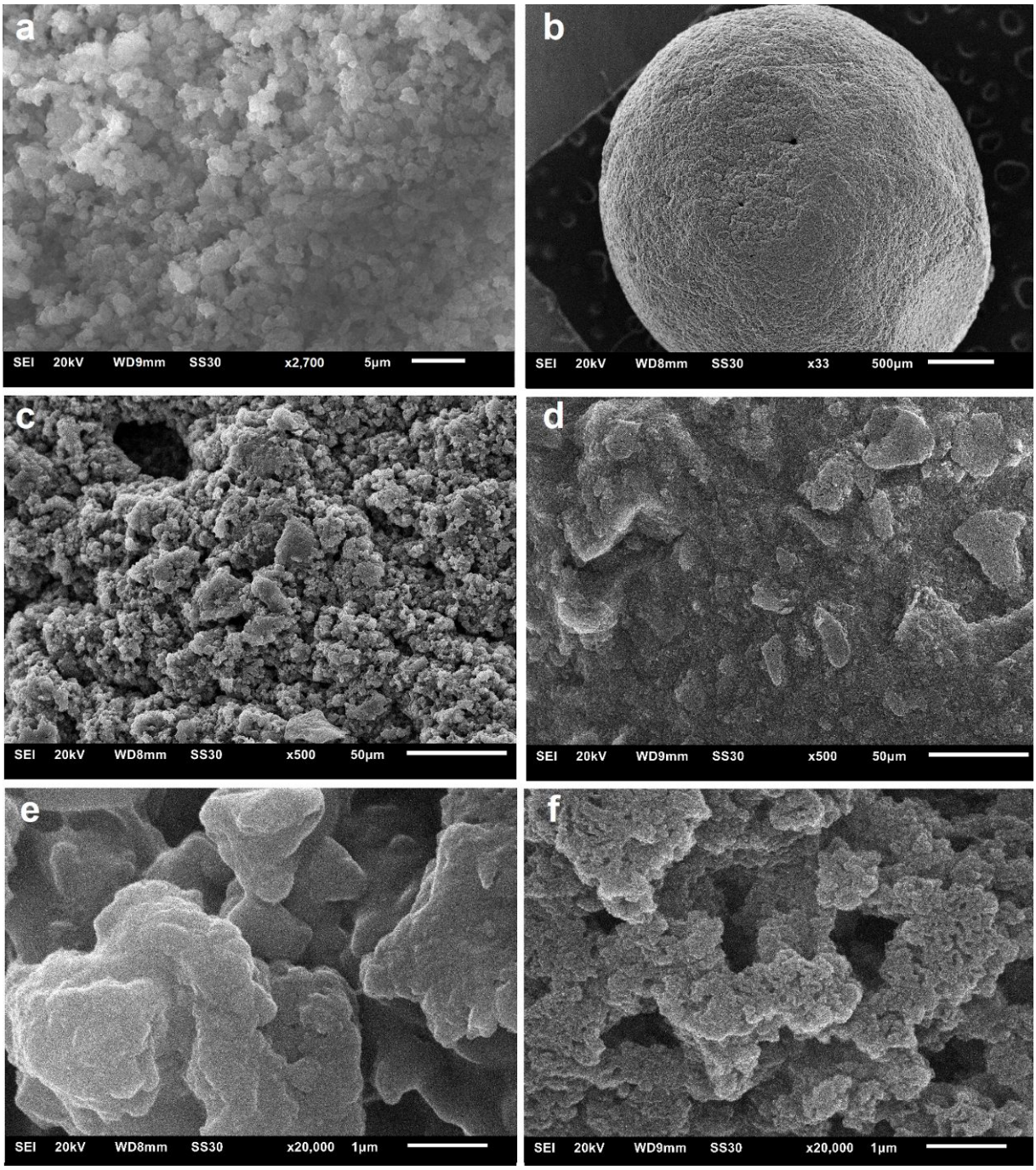

Figure S7 SEM pictures of Al-fum powder (a), overview of Al-fum pellet (b) surface of Al-fum pellet (c, e) and cross section of Al-fum pellet (d, f).

Zr-fum

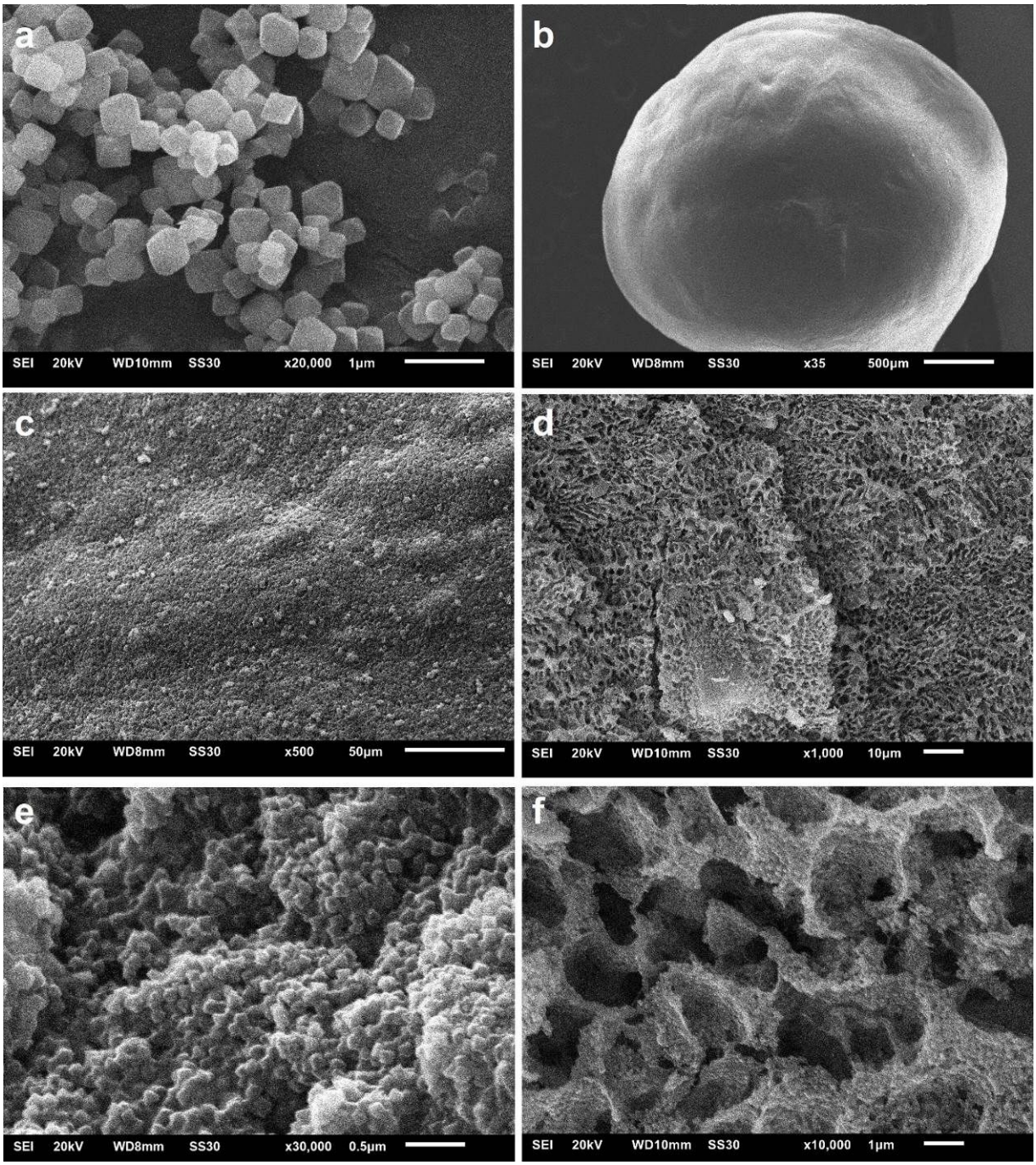

Figure S8 SEM pictures of Zr-fum powder (a), overview of Zr-fum pellet (b), surface of Zr-fum pellet (c, e) and cross section of Zr-fum pellet (d, f). (e) is an enlarged view of SEM-picture of manuscript.

UiO-66

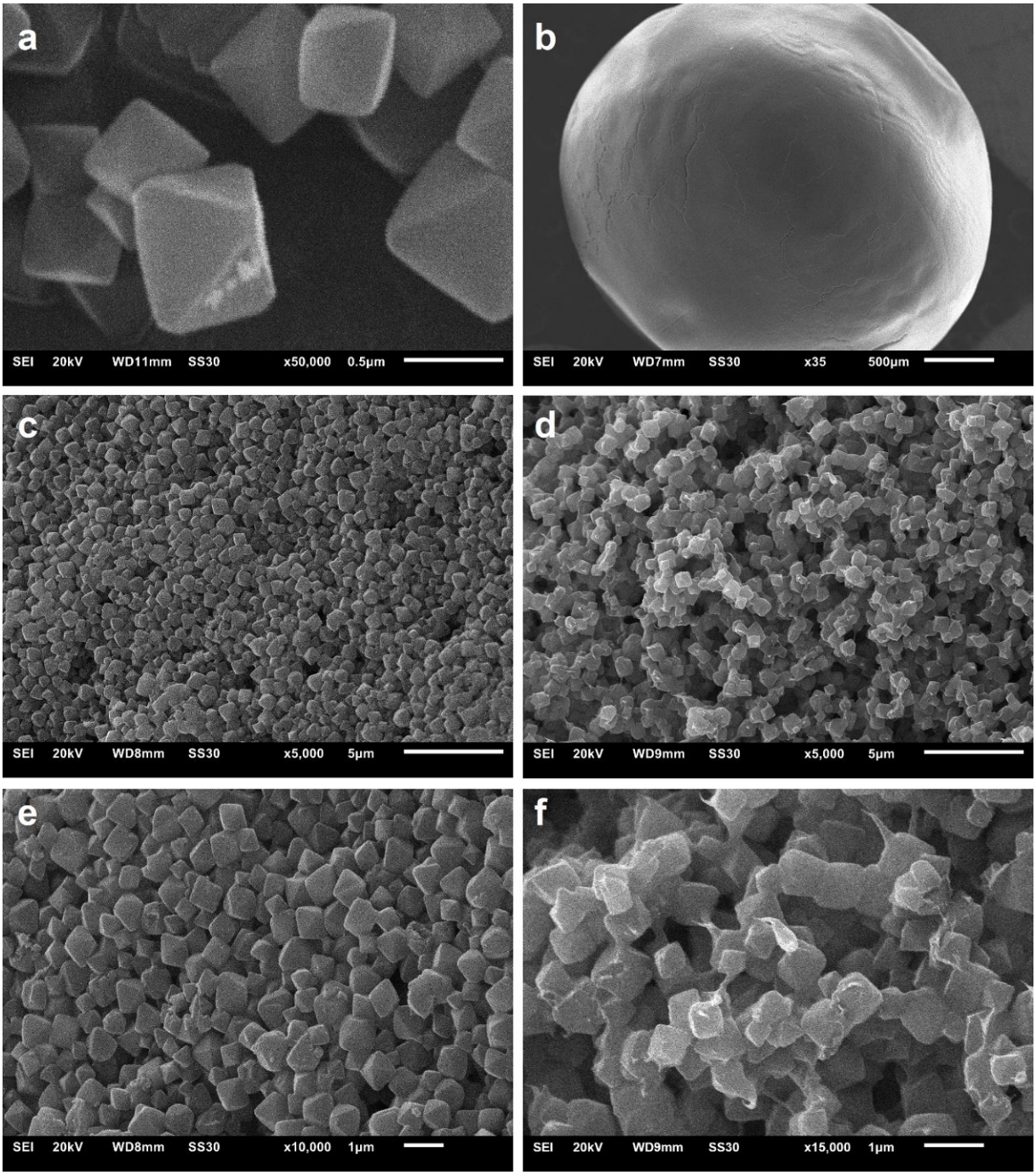

Figure S9 SEM pictures of UiO-66 powder (a), overview of UiO-66 pellet (b), surface of UiO-66 pellet (c, e) and cross section of UiO-66 pellet (d, f). (e) is also given in the manuscript.

Section S7. Water Sorption Cycling: PXRD After 1000 Cycles and N_2 Sorption Before and After 1000 Water Sorption Cycles

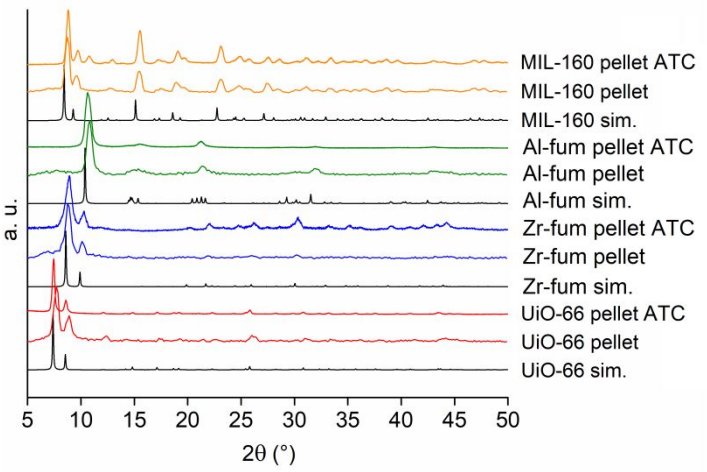

Figure S10 PXRD of MIL-160, Al-fum, Zr-fum and UiO-66 pellets after 1000 ad- and desorption cycles (ATC) of water.

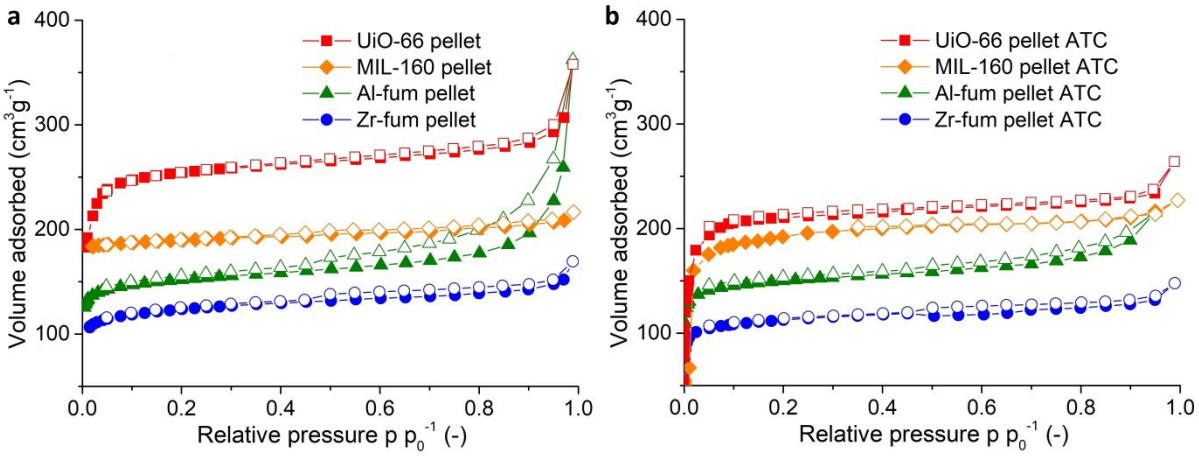

Figure S11 N_2-sorption isotherms of MIL-160, Al-fum, Zr-fum and UiO-66 pellets a) before and b) after 1000 water ad- and desorption cycles.

Table S3 N_2 and water sorption of MIL-160, Al-fum, Zr-fum and UiO-66 pellets before and after 1000 water ad- and desorption cycles.

	N_2 Sorption				Water sorption	
	before 1000 water ad- and desorption cycles		after 1000 water ad- and desorption cycles		before 1000 water ad- and desorption cycles	after 1000 water ad- and desorption cycles
MOF	SBET of pellets [$m^2\ g^{-1}$]	Total pore volume of pellets [b] [$cm^3\ g^{-1}$]	SBET of pellets [$m^2\ g^{-1}$] (% of before cycling)	Total pore volume of pellets [b] [$cm^3\ g^{-1}$] (% of before cycling)	Water uptake at rH of 0.76 [$g\ g^{-1}$]; before cycl. (40°C)	Water uptake of pellets at rH of 0.76 [$g\ g^{-1}$]; after cycl. (40°C)
MIL-160	866	0.32	880 (102)	0.32 (100)	0.30	0.30
Al-fum	595	0.30	593 (100)	0.30 (100)	0.30	0.28
Zr-fum	479	0.22	437 (91)	0.20 (91)	0.25	0.20
UiO-66	1031	0.44	835 (81)	0.35 (80)	0.38	0.28

[b] total pore volume is calculated at $p\ p_0^{-1} = 0.90$ by using Gurvich-rule for pores ≤ 21 nm.

Section S8. Thermogravimetric Analysis (TGA) and Differential Scanning Calorimetry (DSC) of Pellets

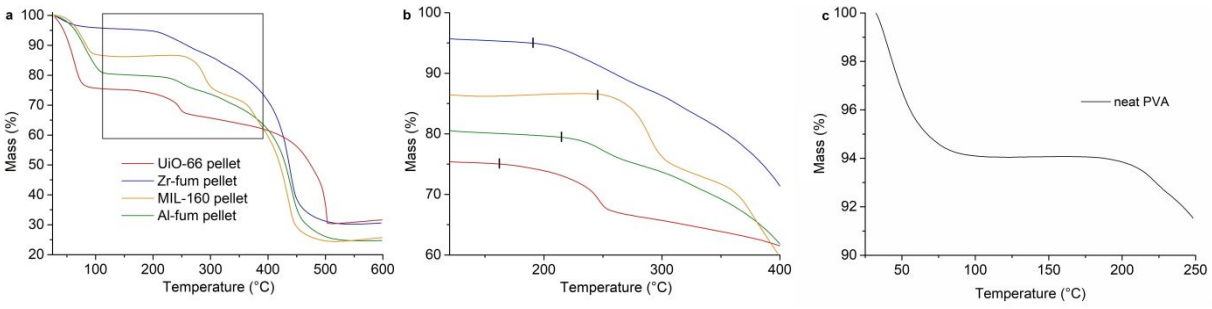

Figure S12 a) Thermogravimetric analysis of MIL-160, Al-fum, Zr-fum and UiO-66 pellets, b) enlarged view of TGA from 120 °C to 400 °C with marked starting points of weight loss debt by PVA and c) thermogravimetric analysis of neat PVA.

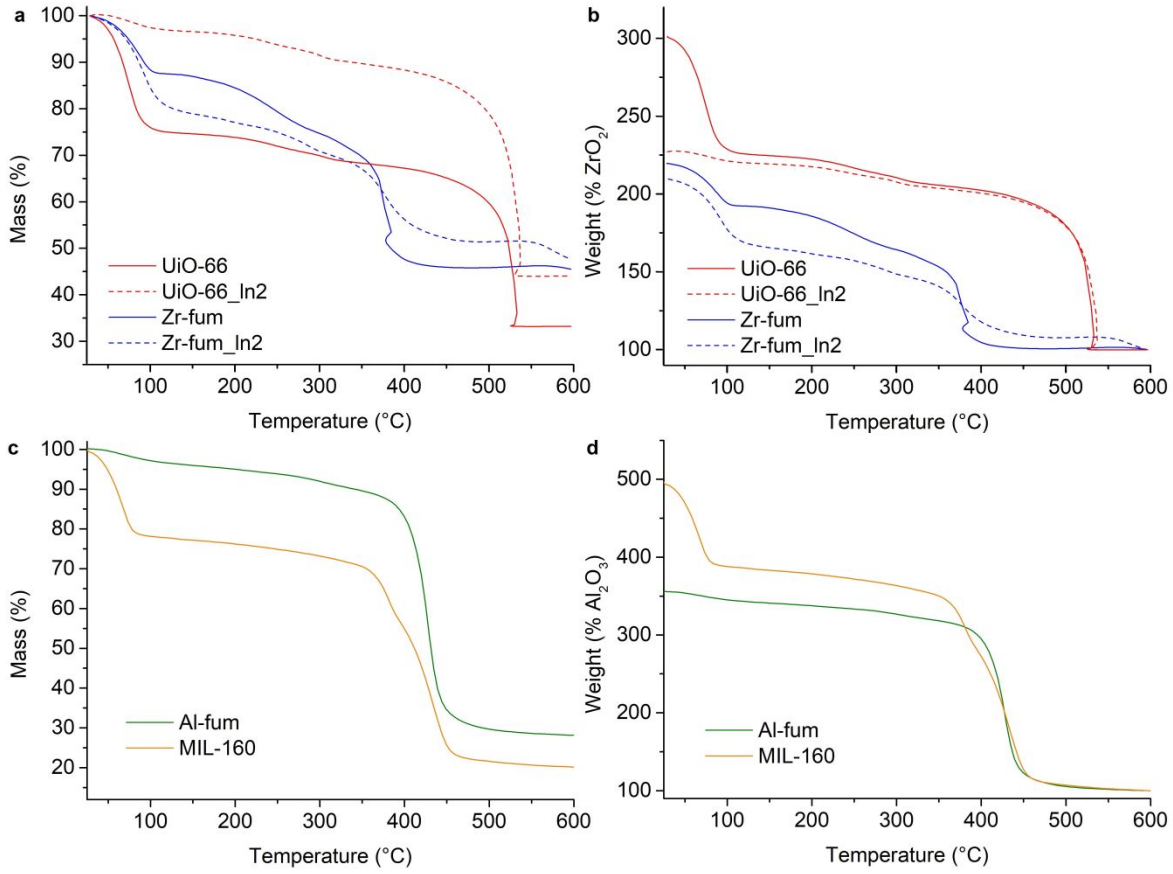

Figure S13 Thermogravimetric analysis of a) Zr-fum and UiO-66 powder (including liquid N_2 treated sample – LN_2) and c) MIL-160 and Al-fum powder; Thermogravimetric analysis are set to end weight of 100% b) ZrO_2 (including LN_2) and d) Al_2O_3.

UiO-66: $Zr_6O_6(C_8H_4O_4)_6 + 45\ O_2 \longrightarrow 6\ ZrO_2 + 48\ CO_2 + 12\ H_2O$

Zr-fum: $Zr_6O_6(C_4H_2O_4)_6 + 18\ O_2 \longrightarrow 6\ ZrO_2 + 24\ CO_2 + 6\ H_2O$

Al-fum: $AlC_4O_5H_3 + 3\ O_2 \longrightarrow 1/2\ Al_2O_3 + 4\ CO_2 + 3/2\ H_2O$

MIL-160: $AlC_6O_6H_3 + 9/2\ O_2 \longrightarrow 1/2\ Al_2O_3 + 6\ CO_2 + 3/2\ H_2O$

First we have to determine theoretical TGA plateau weight $W_{Theo.Plat}$:
$\mathbf{W_{Theo.Plat} = (M_{Comp}/M_{6xZrO2})*W_{End}}$
$\mathbf{W_{Theo.Plat} = (M_{Comp}/M_{1/2xAl2O3})*W_{End}}$

Where:
$\mathbf{M_{Comp}}$ is the molar mass of composition of interest:
M_W(UiO-66) = 1628.03 g/mol
M_W(Zr-fum) = 1327.68 g/mol
M_W(Al-fum) = 158.04 g/mol
M_W(MIL-160) = 198.07 g/mol
$\mathbf{M_{6xZrO2}}$ is the molar mass of 6 moles of zirconium oxide (**739.34** g/mol)
$\mathbf{M_{1/2\ Al2O3}}$ molar mass of 1/2 Al_2O_3 **50.98** g/mol

$\mathbf{W_{End}}$ is the end weight of the TGA run (= **100 %** if normalized as described above).
$\mathbf{W_{Theo.Plat}}$ (UiO-66) = 220 %
$\mathbf{W_{Theo.Plat}}$ (Zr-fum) = 180 %
$\mathbf{W_{Theo.Plat}}$ (Al-fum) = 310 %
$\mathbf{W_{Theo.Plat}}$ (MIL-160) = 389 %

The weight contribution per linker $\mathbf{Wt.PL_{Theo}}$ can be determined by following equation:
$\mathbf{Wt.PL_{Theo} = (W_{Theo.Plat} - W_{End})/NL_{Ideal}}$
$\mathbf{Wt.PL_{Theo}}$ (UiO-66) = (220−100)/6 = 20.03 %
$\mathbf{Wt.PL_{Theo}}$ (Zr-fum) = (180−100)/6 = 13.33 %
$\mathbf{Wt.PL_{Theo}}$ (Al-fum) = (310−100)/1 = 210 %
$\mathbf{Wt.PL_{Theo}}$ (MIL-160) = (389 −100)/1 = 289 %

The experimental number of linkers per SBU, $\mathbf{NL_{Exp}}$ can be determined by following equation:
$\mathbf{NL_{Exp} =(6-x)=(W_{Exp.Plat} - W_{End})/ Wt.PL_{Theo}}$
$\mathbf{NL_{Exp} =(1-x)=(W_{Exp.Plat} - W_{End})/ Wt.PL_{Theo}}$
Where:
$\mathbf{W_{Exp.Plat}}$ is the experimental TGA
$\boldsymbol{x}$ is the number of linker deficiencies per cluster unit and can be determined by following equation:
$\mathbf{x= 6 - NL_{Exp} = 6-((W_{Exp.Plat} - W_{End})/Wt.PL_{Theo})}$
$\mathbf{x= 1 - NL_{Exp} = 1-((W_{Exp.Plat} - W_{End})/Wt.PL_{Theo})}$
x (UiO-66) = 6−4.89= 6−((**198**−100 %)/20.03 %) = **1.11**
x (UiO-66_LN_2) = 6−4.89= 6−((**198**−100 %)/20.03 %) = **1.11**
x (Zr-fum) = 6−4.87 = 6−((**165**−100 %)/13.33 %) = **1.13**
x (Zr-fum_LN_2) = 6−3.60 = 6−((**148**−100 %)/13.33 %) = **2.40**
x(Al-fum) = 1−0.99 = 1−((**308**−100 %)/210 %) = **0.01**
x(MIL-160) = 1−0.88 = 1−((**355**−100 %)/289 %) = **0.12**

The MOFs Alfum and MIL-160 do not have many defects in terms of missing linkers.
The MOF UiO-66 has about one missing linker for each hexanuclear {Zr_6} cluster which is a typically value quite often found in literature.[26,27] The liquid-nitrogen (LN_2) treatment does not affect the linker deficiency in UiO-66.
The as-synthesized MOF Zr-fum initially also has about one missing linker for each hexanuclear {Zr_6} cluster. However, in case of Zr-fum the shaping treatment strongly increases, i.e. more than doubles the linker deficiencies from 1.13 to 2.40.

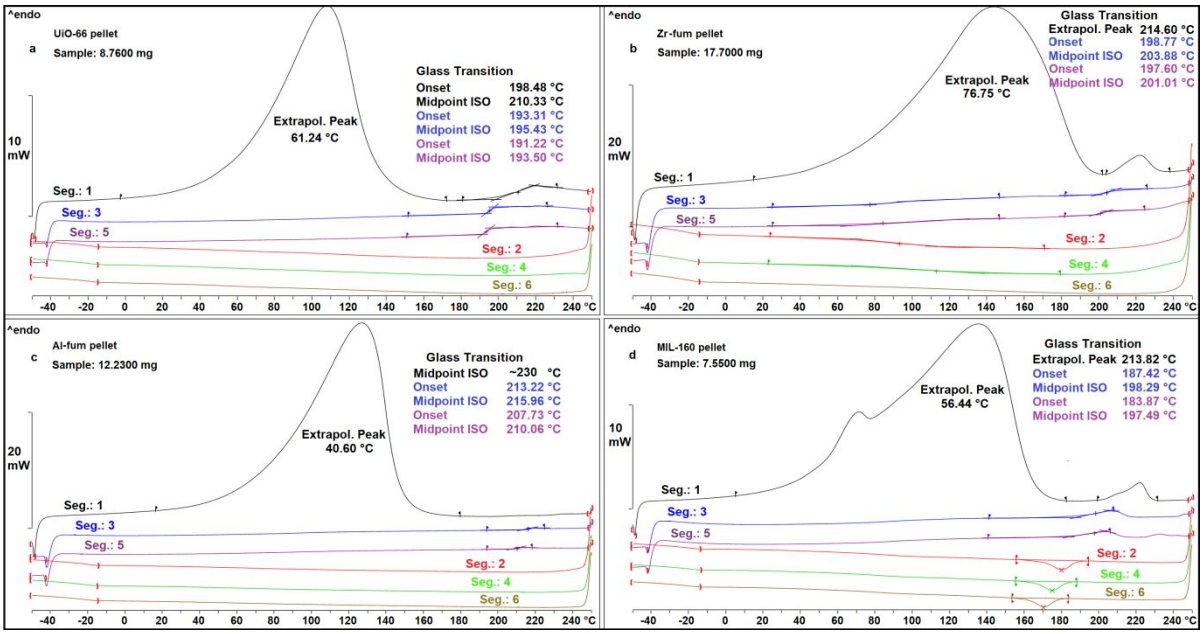

Figure S14 Differential scanning calorimetry of a) UiO-66, b) Zr-fum, c) Al-fum and d) MIL-160 pellets.

Section S9. Hg-Porosimetry

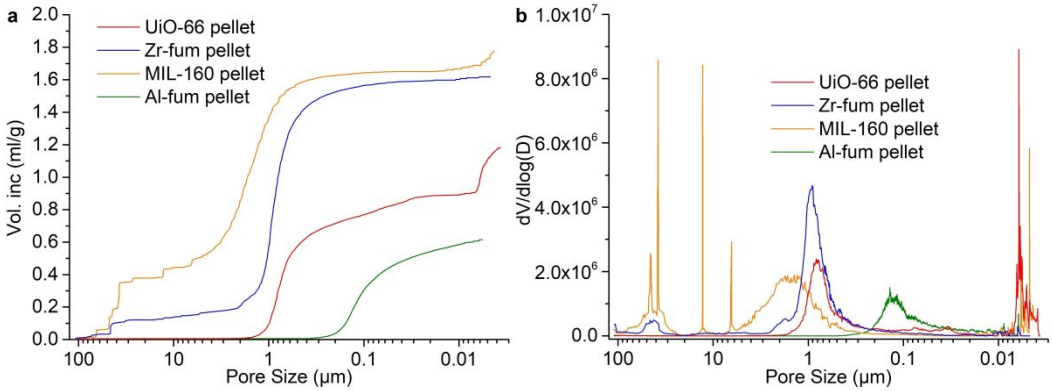

Figure S15 a) Cumulative pore volume and b) pore size distribution resulting from Hg-porosimetry MIL-160, Al-fum, Zr-fum and UiO-66 pellets.

Section S10. The Role of Random Coils During Water Sorption in PVA/MOF Composites and Pellet-Fabrication Set-up

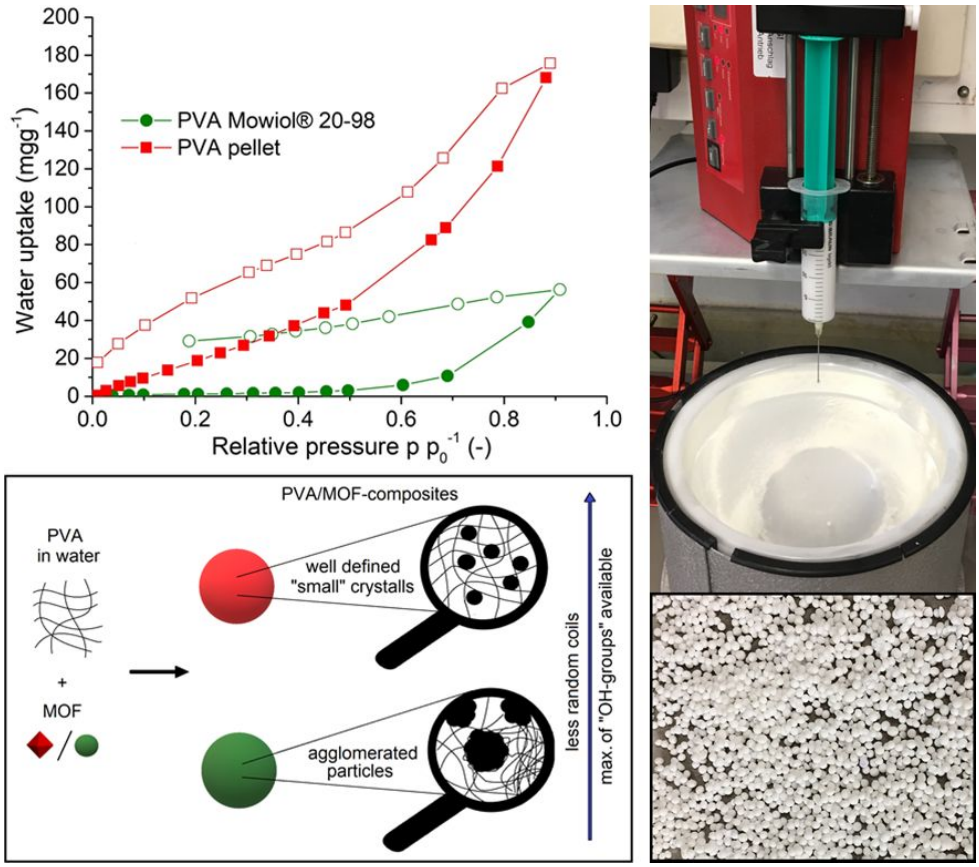

Figure S16 Left: Water sorption of untreated PVA (PVA Mowiol® 20-98) and pure, "freeze granulated"-PVA (PVA pellet) (top) and schematic presentation of availability of OH-groups of PVA depending on particle size of MOF (bottom). Filled symbols adsorption; empty symbols desorption. Water sorption isotherms are measured at 20 °C. Right: Picture of pellet-fabrication process (top) and obtained product (bottom).

Section S11. Characterization of Al-fum Pellets (Large-Scale Synthesis)

Aluminum-based MOFs like MIL-53,[28] Al-fumarate (Alfum, Basolite A520),[10,11] CAU-10-H,[29] and MIL-160[12] can be considered among the most promising MOFs with regard to applications. Al-fum is among the Al-MOFs which exhibit proven hydrothermal stability and water uptake to make them eligible for heat transformation applications. At the same time, it is important for applications that the synthesis and porous properties of these MOFs are robust, that is readily reproducible within certain limits. The synthesis literature on aluminum fumarate is extensive. And indeed, Al-fum can be reproducibly synthesized with robust porosity properties, which are independent of the synthesis method underscoring the potential of these MOFs for applications.[30] Furthermore, the MOF is commercially available, which underlines the importance of aluminum fumarate.

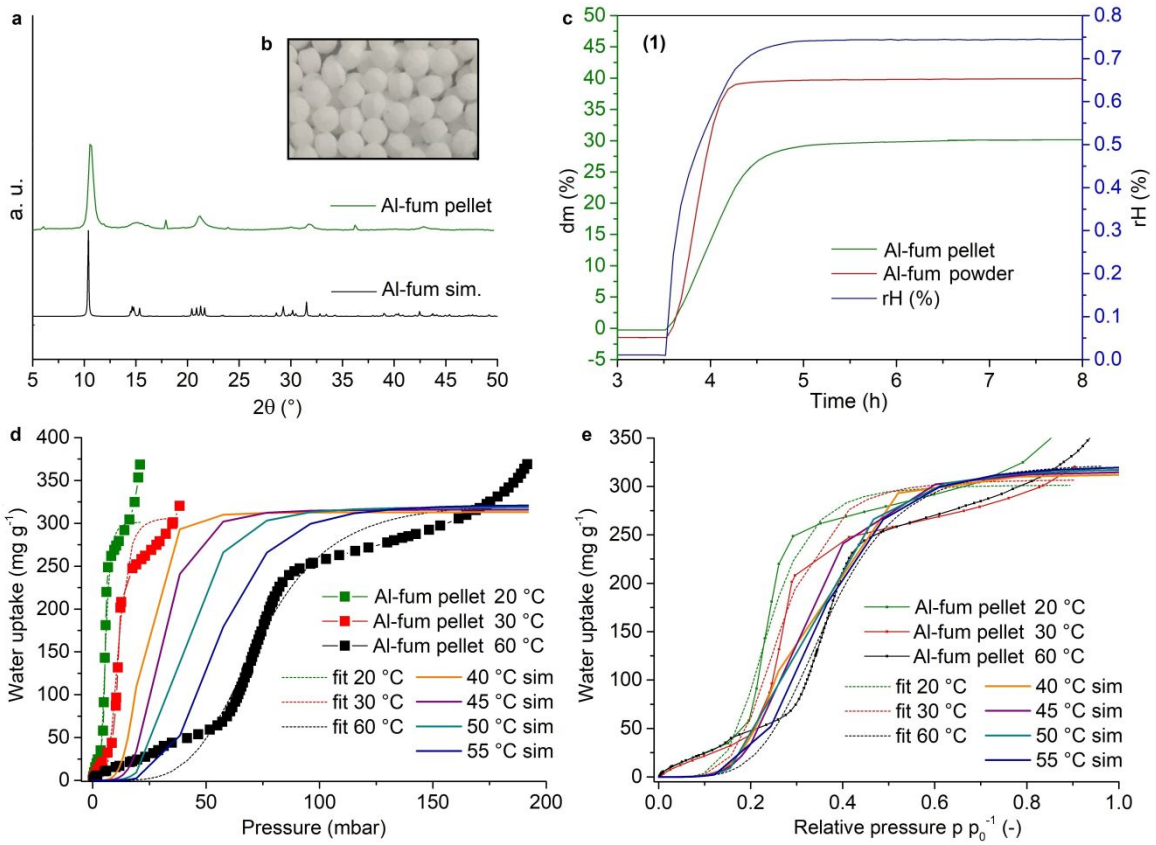

Figure S17 a) XRD of Al-fum pellet (large-scale synthesis) compared to simulated data, b) picture of fabricated pellets, c) Gravimetric water sorption measurements at 40 °C and rH of 74.5% and d) and e) water sorption isotherms of Al-fum pellets at 20 °C, 30 °C and 60 °C and their simulations at 40 °C, 45 °C, 50 °C and 55 °C using SIPS simulations giving calculated heat of adsorption of 52 KJ/mol.

Section S12. Characterization Adsorption Heat Transformation

A home built adsorber element test setup (short «AdElTest«) was used for the measurements under closed conditions. The setup performs pressure jumps at quasi-isothermal adsorption temperatures. Figure S17 shows a schematic representation of the setup. In the test setup the samples (3) are positioned inside a measurement chamber (1) suspended by a scale (2) and connected to the distributor circuit through flexible tubes. The working fluid is provided by a second heat exchanger partially submerged in water (6) working as either evaporator or condenser. It is placed in a second chamber (5) that is connected to the first chamber via two corrugated tubes.

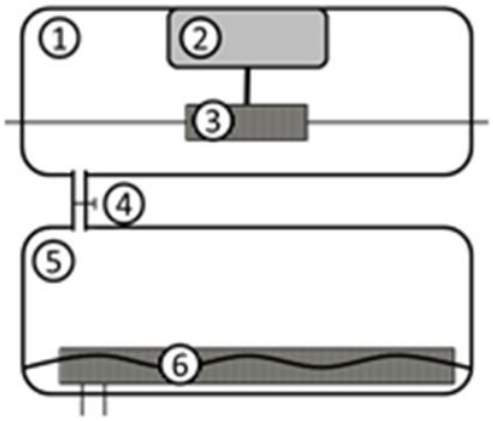

Figure S18 Schematic representation of the test setup used to characterise the full scale adsorber with (1) primary chamber, (2) scale, (3) adsorber with hydraulic connections, (4) valve, (5) secondary chamber, (6) evaporator partially submerged in water.[31]

The measurement procedure is presented in Figure S18. Prior to measurements, the adsorbent was desorbed at elevated temperature and vacuum (90°C, 6 h) and let cool down to adsorption temperature T_M (step A). The evaporator was then set to evaporation temperature T_{evap}. The adsorber was preloaded to a target loading via incremental dosage of small amounts of water vapor from the evaporator to the primary chamber (step B). When the conditioning of the adsorber is completed and the starting pressure (p_{init}) is reached in the primary chamber, the adsorption phase was started by completely opening the valve between chamber 1 and 2 (step C). In a variation, the experiment was conducted by initiating the adsorption directly from the evacuated state (step B').

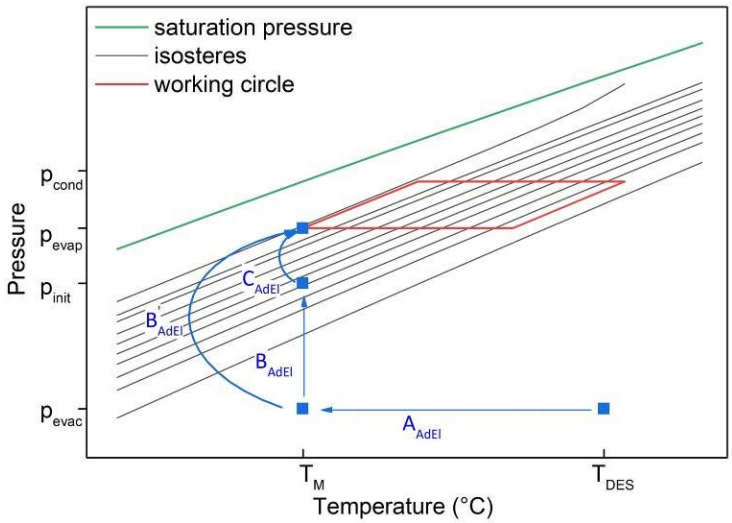

Figure S19 Schematic description of measuring procedure for the full scale AdsHX. First, the sample is desorbed at 90°C under vacuum, then let cool down to measurement temperature (A). Afterwards it was either preloaded (B) before the pressure jump for the measurement (C) was performed or a pressure jump was performed directly from the evacuated state (B').

Methods: The change in loading over time is the central parameter to evaluate adsorption kinetics. A central key data is the adsorption speed v_{ads}. It is calculated by dividing the loading difference ΔX by time. Different characteristic times are used in literature. Herein used is the time t_{90}, representing the time, in which 90% of the end loading is reached.
Different characteristic values for the power evaluation can be determined by means of energy balance in the adsorption circuit, time and geometric dimensions. It is important to notice that the experiment is a pressure jump method, where the sorber is quasi-isothermal. Therefore, the sensible heat of the

sorber has little effect to the power output. This is a big difference to cycle measurements, where the adsorption power output is always higher due to the sensible heat released.
The mean cooling power is calculated from the scale signal and a constant evaporation enthalpy for the characteristic time t_{90}.

$$\overline{\dot{Q}_{cool}} = \frac{m_{uptake}}{t} \cdot 2500 \frac{kJ}{kg} \quad (1)$$

The cooling power is calculated from the derivative of the integral heat of evaporation:

$$P_{Cool} = \frac{d}{dt}\left[m_{Ads}(t) \cdot 2500 \frac{kJ}{kg}\right] \quad (2)$$

For better comparison volume-specific values are presented for power. The main key data is listed in Table S3. The test parameters and different weights are listed in Table S4 and Table S5.

Table S4. Main key data.

Item	Unit	Description
m_{sorb}	kg	dry mass of sorbent on HX
v_{ads}	$\cdot 10^{-4} \frac{g}{g \cdot s}$	adsorption speed
$\dot{Q}_{ads}$	W	mean specific adsorption power from energy balance
h_{ads}	$\frac{kJ}{kg}$	adsorption enthalpy
$\dot{Q}_{cool}$	W	mean specific cooling power via water uptake and enthalpy

Table S5. Parameter for AdEl tests.

Item	Unit	Data set real(target) – 1	Data set real(target) – 2
Desorption temperature	°C	90°C	60
Adsorption temperature	°C	30°C	22
Evaporation temperature	°C	18°C	18
Volume flow adsorber circuit	l/min	10	
Volume flow evaporator circuit	l/min	10	
Initial pressure p_{mc}	mbar	2.14	3.18

Table S6. Weights and volume of module.

	Weight or Volume
Heat exchanger	2388 g
Copper mesh	1289 g
Stainless steel frame	1421 g
Mass of adsorbent (desorbed)	334 g
Heat exchanger volume	2.34 L

Section S13. References

(1) Cavka, J. H.; Jakobsen, S.; Olsbye, U.; Guillou, N.; Lamberti, C.; Bordiga, S.; Lillerud, K. P. A New Zirconium Inorganic Building Brick Forming Metal Organic Frameworks with Exceptional Stability. *J. Am. Chem. Soc.* **2008**, *130*, 13850–13851.
(2) Wißmann, G.; Schaate, A.; Lilienthal, S.; Bremer, I.; Schneider A. M.; Behrens, P. Modulated synthesis of Zr-fumarate MOF. *Microporous Mesoporous Mater.* **2012**, *152*, 64–70.
(3) Wu, H.; Chua, Y. S.; Krungleviciute, V.; Tyagi, M.; Chen, P.; Yildirim, T.; Zhou, W. Unusual and Highly Tunable Missing-Linker Defects in Zirconium Metal–Organic Framework UiO-66 and Their Important Effects on Gas Adsorption. *J. Am. Chem. Soc.* **2013**, *135*, 10525−10532.
(4) Anjum, M. W.; Vermoortele, F.; Khan, A. L.; Bueken, B.; De Vos, D. E.; Vankelecom, I. F. J. Modulated UiO-66-Based Mixed-Matrix Membranes for CO_2 Separation. *ACS Appl. Mater. Interfaces* **2015**, *7*, 25193–25201.
(5) Jeremias, F.; Lozan, V.; Henninger, S. K.; Janiak, C. Programming MOFs for Water Sorption: Amino-Functionalized MIL-125 and UiO-66 for Heat Transformation and Heat Storage Applications. *Dalton Trans.* **2013**, *42*, 15967−15973.
(6) Jeremias, F.; Fröhlich, D.; Janiak, C.; Henninger, S. Water and Methanol Adsorption on MOFs for Cycling Heat Transformation Processes. *New J. Chem.* **2014**, *38*, 1846–1852.
(7) Shahat, A.; Hassan, H. M. A.; Azzazy, H. M. E. Optical Metal-Organic Framework Sensor for Selective Discrimination of Some Toxic Metal Ions in Water. *Analyt. Chim. Acta* **2013**, *793*, 90–98.
(8) Vermoortele, F.; Bueken, B.; Le Bars, G.; Van de Voorde, B.; Vandichel, M.; Houthoofd, K.; Vimont, A.; Daturi, M.; Waroquier, M.; Van Speybroeck, V.; Kirschhock, C.; De Vos, D. E. Synthesis Modulation as a Tool to Increase the Catalytic Activity of Metal–Organic Frameworks: The Unique Case of UiO-66 (Zr). *J. Am. Chem. Soc.* **2013**, *135*, 11465–11468.
(9) Valenzano, L.; Civalleri, B.; Chavan, S.; Bordiga, S.; Nilsen, M. H.; Jakobsen, S.; Lillerud, K. P.; Lamberti, C.; Disclosing the Complex Structure of UiO-66 Metal Organic Framework: A Synergic Combination of Experiment and Theory. *Chem. Mater.* **2011**, *23*, 1700–1718.
(10) Leung, E.; Müller, U.; Trukhan, N.; Mattenheimer, H.; Cox, G.; Blei, S. Process for Preparing Porous Metal-Organic Frameworks Based on Aluminum Fumarate. *US8524932B2, US20120082864* **2013**.
(11) Alvarez, E.; Guillou, N.; Martineau, C.; Bueken, B.; Van de Voorde, B.; Le Guillouzer, C.; Fabry, P.; Nouar, F.; Taulelle, F.; de Vos, D.; Chang, J.-S.; Cho, K. H.; Ramsahye, N.; Devic, T.; Daturi, M.; Maurin, G.; Serre, C. The Structure of the Aluminum Fumarate Metal–Organic Framework A520. *Angew. Chem. Int. Ed.* **2015**, *54*, 3664–3668.
(12) Cadiau, A.; Lee, J. S.; Borges, D. D.; Fabry, P.; Devic, T.; Wharmby, M. T.; Martineau, C.; Foucher, D.; Taulelle, F.; Jun, C.-H.; Hwang, Y. K.; Stock, N.; De Lange, M. F.; Kapteijn, F.; Gascon, J.; Maurin, G.; Chang J.-S.; Serre, C. Design of Hydrophilic Metal Organic Framework Water Adsorbents for Heat Reallocation. *Adv. Mater.* **2015**, *27*, 4775–4780.
(13) Permyakova, A.; Skrylnyk, O.; Courbon, E.; Affram, M.; Wang, S.; Lee, U-H.; Valekar, A. H.; Nouar, F.; Mouchaham, G.; Devic, T.; Weireld, G. D.; Chang, J.-S.; Steunou, N.; Frere, M.; Serre, C. Synthesis Optimization, Shaping, and Heat Reallocation Evaluation of the Hydrophilic Metal–Organic Framework MIL-160(Al). *ChemSusChem* **2017**, *10*, 1419–1426.
(14) Wahiduzzaman, M.; Lenzen, D.; Maurin, G.; Stock, N.; Wharmby, M. T. Rietveld Refinement of MIL-160 and its Structural Flexibility upon H_2O and N_2 Adsorption. *Eur. J. Inorg. Chem.* **2018**, 3626–3632.
(15) Kim, S.-N.; Lee, Y.-R.; Hong, S.-H.; Jang M.-S.; Ahn, W.-S; Pilot-Scale Synthesis of a Zirconium-Benzenedicarboxylate UiO-66 for CO_2 Adsorption and Catalysis. *Catal. Today* **2015**, *245*, 54–60.

(16) Khabzina, Y.; Dhainaut, J.; Ahlhelm, M.; Richter, H.-J.; Reinsch, H.; Stock, N.; Farrusseng, D. Synthesis and Shaping Scale-up Study of Functionalized UiO-66 MOF for Ammonia Air Purification Filters. *Ind. Eng. Chem. Res.* **2018**, *57*, 8200–8208.
(17) Valekar, A. H.; Cho, K.-H.; Lee, U.-H.; Lee, J. S.; Yoon, J. W.; Hwang, Y. K.; Lee, S. G.; Cho S. J.; Chang, J.-S.; Shaping of Porous Metal–Organic Framework Granules Using Mesoporous ρ-Alumina as a Binder. *RSC Adv.* **2017**, *7*, 55767–55777.
(18) Lenzen, D.; Bendix, P.; Reinsch, H.; Fröhlich, D.; Kummer, H.; Möllers, M.; Hügenell, P. P. C.; Gläser, R.; Henninger, S. K.; Stock, N. Scalable Green Synthesis and Full-Scale Test of the Metal–Organic Framework CAU-10-H for Use in Adsorption-Driven Chillers. *Adv. Mater.* **2017**, *6*, 1705869.
(19) Ren, J.; Musyoka, N. M.; Langmi, H. W.; Swartbooi, A.; North, B. C.; Mathe, M.; A More Efficient Way to Shape Metal-Organic Framework (MOF) Powder Materials for Hydrogen Storage Applications. *Int. J. Hydrogen Energ.* **2015**, *40*, 4617–4622.
(20) Moreira, M. A.; Santos, J. C.; Ferreira, A. F. P.; Loureiro, J. M.; Ragon, F.; Horcajada, P.; Shim, K.-E.; Hwang, Y.-K.; Lee, U.-H.; Chang, J.-S.; Serre, C.; Rodrigues, A. E.*;* Reverse Shape Selectivity in the Liquid-Phase Adsorption of Xylene Isomers in Zirconium Terephthalate MOF UiO-66. *Langmuir* **2012**, *28*, 5715−5723.
(21) Pinto, M. L.; Dias, S.; Pires, J.; Composite MOF Foams: The Example of UiO-66/Polyurethane. *ACS Appl. Mater. Interfaces* **2013**, *5*, 2360–2363.
(22) Li, L.; Yao, J.; Xiao, P.; Shang, J.; Feng, Y.; Webley, P. A.; Wang, H.; One-Step Fabrication of ZIF-8/Polymer Composite Spheres by a Phase Inversion Method for Gas Adsorption. *Colloid Polym. Sci.* **2013**, *291*, 2711–2717.
(23) Jeremias, F.; Khutia, A.; Henninger, S. K. Janiak, C. MIL-100(Al, Fe) as water adsorbents for heat transformation purposes—a promising application. *J. Mater. Chem.* **2012**, 10148–10151.
(24) Jeremias, F.; Lozan, V.; Henninger, S. K.; Janiak, C. Programming MOFs for water sorption: amino-functionalized MIL-125 and UiO-66 for heat transformation and heat storage applications. *Dalton Trans.* **2013**, *42*, 15967–15973.
(25) Fröhlich, D.; Pantatosaki, E.; Kolokathis, P. D.; Markey, K.; Reinsch, H.; Baumgartner, M.; van der Veen, M. A.; De Vos, D. E.; Stock, N.; Papadopoulos, G. K.; Henninger, S. K.; Janiak, C. Water Adsorption Behaviour of CAU-10-H: A Thorough Investigation of Its Structure–Property Relationships. *J. Mater. Chem. A* **2016**, *4*, 11859–11869.
(26) Shearer, G. C.; Chavan, S.; Bordiga, S.; Svelle, S.; Olsbye, U.; Lillerud, K. P. Defect Engineering: Tuning the Porosity and Composition of the Metal–Organic Framework UiO-66 via Modulated Synthesis. *Chem. Mater.* **2016**, *28*, 3749–3761.
(27) Gökpinar, S.; Diment, T.; Janiak, C. Environmentally Benign Dry-Gel Conversions of Zr-Based UiO Metal–Organic Frameworks With High Yield and the Possibility of Solvent Re-Use. *Dalton Trans.* **2017**, *46*, 9895-9900.
(28) Millange, F.; Serre, C.; Férey, G. Synthesis, Structure Determination and Properties of MIL-53as and MIL-53ht: The First CrIII Hybrid Inorganic–Organic Microporous Solids: CrIII(OH)·{O2C–C6H4–CO2}·{HO2C–C6H4–CO2H}x. *Chem. Commun.* **2002**, 822–823.
(29) Reinsch, H.; van der Veen, M. A; Gil, B.; Marszalek, B.; Verbiest, T.; de Vos D.; Stock, N. Structures, Sorption Characteristics, and Nonlinear Optical Properties of a New Series of Highly Stable Aluminum MOFs. *Chem. Mater.* **2013**, 25, 17-26.
(30) Tannert, N.; Jansen, C.; Nießing, S.; Janiak, C. Robust Synthesis Routes and Porosity of the Al-based Metal–Organic Frameworks Al-fumarate, CAU-10-H and MIL-160. *Dalton Trans.* **2019**, *48*, 2967–2976.
(31) Bendix, P.; Füldner, G.; Möllers, M.; Kummer, H.; Schnabel, L.; Henninger, S.; Henning, H.-M.; Optimization of Power Density and Metal-to-Adsorbent Weight Ratio

in Coated Adsorbers for Adsorptive Heat Transformation Applications. *Appl. Therm. Eng.* **2017**, *124*, 83–90.